Mingchao Wang, Mao Wang, Hung-Hsuan Lin, Marco Ballabio, Haixia Zhong, Mischa Bonn, Shengqiang Zhou, Thomas Heine, Enrique Cánovas*, Renhao Dong*, and Xinliang Feng

# High-Mobility Semiconducting Two-Dimensional Conjugated Covalent Organic Frameworks with p-Type Doping

**Erstveröffentlichung in / First published in:**

*Journal of the American Chemical Society.* 2020, 142 (52), S. 21622–21627 [Zugriff am: 20.12.2021]. ACS Publications. ISSN 1520-5126.

DOI: https://doi.org/10.1021/jacs.0c10482

Final edited form was published in "Journal of the American Chemical Society". 2020, 142 (52), S. 21622–21627. ISSN 1520-5126.
https://doi.org/10.1021/jacs.0c10482

# High-Mobility Semiconducting Two-Dimensional Conjugated Covalent Organic Frameworks with *p*-Type Doping

Mingchao Wang,[†,⊥] Mao Wang,[‡,⊥] Hung-Hsuan Lin,[†,⊥] Marco Ballabio,[§] Haixia Zhong,[†] Mischa Bonn,[§] Shengqiang Zhou,[‡] Thomas Heine,[†] Enrique Cánovas,*[,§,#] Renhao Dong,*[,†] Xinliang Feng*[,†]

[†]*Center for Advancing Electronics Dresden (cfaed) and Faculty of Chemistry and Food Chemistry, Technische Universität Dresden, Mommsenstrasse 4, 01062 Dresden, Germany*

[‡]*Institute of Ion Beam Physics and Materials Research, Helmholtz-Zentrum Dresden-Rossendorf, Bautzner Landstr. 400, 01328 Dresden, Germany*

[§]*Max Planck Institute for Polymer Research, Ackermannweg 10, 55128 Mainz, Germany*

[#]*Instituto Madrileño de Estudios Avanzados en Nanociencia (IMDEA Nanociencia), Faraday 9, 28049 Madrid, Spain.*

**ABSTRACT:** Two-dimensional conjugated covalent organic frameworks (2D *c*-COFs) are emerging as a unique class of semiconducting 2D conjugated polymers for (opto)electronics and energy storage. Doping is one of the common, reliable strategies to control the charge carrier transport properties, however, the precise mechanism underlying COF doping has remained largely unexplored. Here, we demonstrate a molecular iodine-doping of metal-phthalocyanine-based pyrazine-linked 2D *c*-COF. The resultant **ZnPc-pz-I₂** 2D *c*-COF maintains the structural integrity and displays an enhanced conductivity by 3 orders of magnitude, which is the result of elevated carrier concentrations. Remarkably, Hall effect measurements reveal enhanced carrier mobility reaching ~22 $cm^2/(Vs)$ for **ZnPc-pz-I₂**, which represents a record value for 2D *c*-COFs in both direct and alternating current limits (DC- and AC-limits). This unique transport phenomenon with largely increased mobility upon doping can be traced to increased scattering time for free charge carriers, indicating that scattering mechanisms limiting the mobility are mitigated by doping. Our work provides a guideline on how to assess doping effects in COFs and highlights the potential of 2D *c*-COFs for displaying high conductivities and mobilities towards novel (opto)electronic devices.

Two-dimensional conjugated covalent organic frameworks (2D *c*-COFs)[1] have recently emerged as a unique class of 2D conjugated polymers[2] that display high in-plane $\pi$-conjugation[3] and weak out-of-plane interactions.[4] Owing to their tailorable architectures,[5] abundant active sites,[6] well-defined structures,[7] inherent porosity,[8] chemical stability,[9] and (opto)electronic properties,[10] these materials are promising for chemiresistor,[3b] logic and memory devices,[11] and energy storage.[12] For many of these applications, long-range charge transport is required. As such, much effort has been devoted over the last years to interrogate the nature of the conductivity in 2D *c*-COFs. Recent studies demonstrated charge carrier mobilities ranging from 5 to 8 $cm^2/(Vs)$.[3a,3c,13] Although these mobilities are encouraging, their conductivities have remained rather low (typically $<10^{-6}$ S/cm).[1d,3c] To further improve the conductivity, doping strategies have been employed by incorporating guest molecules acting as dopants, e.g. linear conducting polymers,[12] $C_{60}$,[3a] iodine ($I_2$),[1d,14] etc. For instance, $I_2$-doping has demonstrated improvement in conductivities up to 3 orders of magnitude, however, this approach was often associated with amorphization/irreversible structural changes of 2D *c*-COFs.[14a] A fundamental understanding of the doping interaction within the lattice in COFs remains largely unexplored.

Herein, we demonstrate a doping-defined, polycrystalline 2D *c*-COF (**ZnPc-pz-I₂**) through molecular $I_2$-doping of metal-phthalocyanine-based pyrazine-linked ZnPc-pz 2D *c*-COF. $I_2$-molecules sit preferentially in the COF pores and near the skeleton. Hall effect measurements reveal that doping improves the conductivity and carrier density by approximately 3 and 2 orders of magnitude respectively in **ZnPc-pz-I₂**. Notably, doping also leads to an unprecedented improvement in the Hall mobility from ~5 to ~22 $cm^2/(Vs)$. Employing density functional theory (DFT) and time-resolved terahertz spectroscopy (TRTS), this record mobility is related to an increase of scattering time after doping, likely related to the formation of ordered pathways for the charge carrier migration between the electron donor (ZnPc-pz) and acceptor ($I_2$) within the framework. Such unique phenomena have never been reported among doped COF materials. Our work highlights the potential of developing structurally-defined, doped 2D *c*-COFs with high conductivity and high mobility, which provides insight on a fundamental understanding of the dopant role and the host-dopant interplay necessary to elucidate structure-electronic property relationships.

**ZnPc-pz-I₂** 2D *c*-COF was synthesized by placing dark-green ZnPc-pz powder in $I_2$-vapor, followed by heating at 50 °C under vacuum to remove any excess of aggregated $I_2$. The resultant black sample contains 9-10 wt% $I_2$ as estimated by gravimetric and thermogravimetric analysis (Figure S1), and this estimate corresponds to nearly one $I_2$ molecule per structural unit (Figure 1a, $C_{80}H_{52}N_{16}Zn{\cdot}I_2$). Compared with heavily doped systems with large contents of $I_2$ (>50 wt%) or significantly reduced surface-area,[14] minor amount of dopants is beneficial to accurately probe their effect on the charge transport phenomenon. Powder X-ray diffraction (PXRD) pattern was evaluated for undoped[3c] and doped samples with distinct (100) peaks at ~4.0° (Figure 1b). No obvious change in crystallographic phases was observed after doping. **ZnPc-pz-I₂** retained a AA-

Final edited form was published in "Journal of the American Chemical Society". 2020, 142 (52), S. 21622–21627. ISSN 1520-5126.
https://doi.org/10.1021/jacs.0c10482

serrated stacking model with a=b=22.2 Å. Nevertheless, the intensity of its (100) peak sharply decreased due to the existence of amorphous $I_2$ molecules. Figure 1b also presents calculated patterns when considering the different structural configurations sketched in Figure 1a: $I_2$@1, $I_2$@2, $I_2$@3, $I_2$@4, $I_2$@5, which correlate with $I_2$ molecule located at the center of the pore, close to the backbone, on the porous skeleton, on metal, or on pyrene unit, respectively (Figure S2). Apparently, the experimental PXRD pattern could be reproduced well with the structural models of $I_2$@2 and $I_2$@4. Notably, the diffraction peaks at ~26.7° indicate the same interlayer distance of ~3.30 Å for **ZnPc-pz-I₂** and ZnPc-pz, suggesting that $I_2$ is not likely placed between layers of ZnPc-pz ($I_2$@4/5).

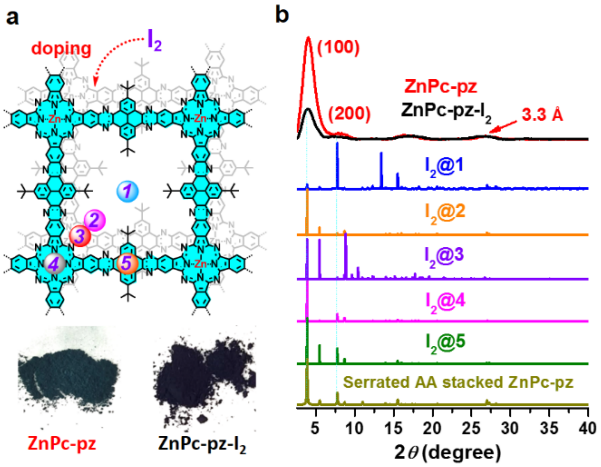


**Figure 1.** (a) Schematic illustration of doping ZnPc-pz with $I_2$. (b) Experimental (black) and calculated PXRD patterns of **ZnPc-pz-I₂** with ZnPc-pz (red) as reference.[3c]

To clarify the influence of doping on structure, we further performed multi-scaled analysis on **ZnPc-pz-I₂**. The porosity was investigated by the nitrogen adsorption measurement, which reveals a declined surface-area of 225 $m^2/g$ (Figure 2a), in contrast to 487 $m^2/g$ for ZnPc-pz.[3c] Both the declined pore volume and increased weight account for the decrement of surface-area. The average pore size was ~1.4 nm. Scanning electron microscopy and energy-dispersive X-ray (EDX) images suggest a homogeneous element distribution over the particle surfaces (Figures S3). Fourier-transform infrared (FT-IR) analysis displays stretching vibration-bands of pyrazine and other resonances consistent with the spectrum of ZnPc-pz (Figure S4). Raman spectrum shows the peaks from ZnPc-pz with an additional one at 172 $cm^{-1}$ for the adsorbed $I_2$ (Figure S6).[15] The C-N vibration-bands at 1413 and 1512 $cm^{-1}$ vary after doping, which implies that at least part of $I_2$ is interacting with the polymer framework. To probe the interactions, we conducted X-ray photoelectron spectroscopy (XPS). Deconvolution of the I($3d_{5/2}$) signal generates peaks at 620.1 and 618.8 eV, attributable to the unassociated and partially charged $I_2$, with peak areas of 19.4 and 80.6%, respectively (Figure 2b and 2c). The C(*1s*) signal is insensitive to doping, while positively shifted N(*1s*) and Zn(*2p*) peaks were observable (Figure S5). Deconvolution of N(*1s*) signal (Figure 2c, down) reveals an additional type of N atom at 400.6 eV, which can be attributed to partial negative charge from ZnPc-pz being transferred to $I_2$, and correlates with the $I_2$@2 configuration for a short distance between $I_2$ and N/Zn atom. Nevertheless, we could not exclude a trace of $I_2$ possibly adsorbed on the surface metal centers of COF particles.

We further investigated de-doping by washing **ZnPc-pz-I₂** with 3 liter dichloromethane. EDX spectroscopy and Raman spectra confirmed the entire elimination of $I_2$ (Figures S6-8). PXRD indicated the structural recovery of pristine ZnPc-pz (Figure S9). These analyses demonstrate no chemical bond formation between ZnPc-pz and $I_2$ in **ZnPc-pz-I₂** that differs from the chemical oxidation upon $I_2$-doping in previous reports.[1d,14,16] DFT calculations indicate that $I_2$@2 is energetically more favorable than $I_2$@1, while $I_2$@3 is the most unstable one (Table S1). The above characterizations shed some light into the potential configuration of $I_2$, with $I_2$@2 being the most plausible.

Surprisingly, ultraviolet-visible-near IR (UV-vis-NIR) absorption spectrum of a dispersion of ZnPc-pz and $I_2$ in dimethyl sulfoxide reveals no evidence of charge-transfer (Figure S10). To eliminate potential effect coming from dimethyl sulfoxide, ZnPc-pz was deposited onto a quartz substrate and doped in the solid-state. A charge-transfer absorption peak centered at 986 nm appeared (Figure 2d), which manifests that **ZnPc-pz-I₂** contains weakly associated electron-donor (ZnPc-pz)-acceptor ($I_2$) pairs,[16] thereby resulting the color change from dark-green to black (Figure 1a). Further evidence comes from the disappearance of this peak for the de-doped sample (Figure S11), suggesting a reversible doping-dedoping process. The derived tauc plots suggest a subtle shift of the optical bandgap from ~1.1 to ~1.0 eV after doping (Figure 2d, left inset).

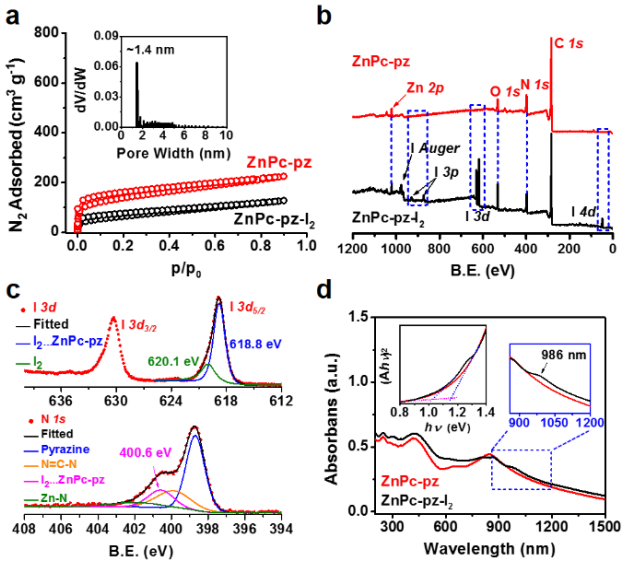


**Figure 2.** (a) Nitrogen adsorption/desorption isotherms with ZnPc-pz[3c] as reference. (b) XPS survey spectra of ZnPc-pz[3c] and **ZnPc-pz-I₂**. (c) High-resolution N(*1s*) and I(*3d*) XPS spectra. (d) UV-vis-NIR spectroscopy of quartz-supported samples.

Next, DFT was employed for calculating the energy band structure for different models (Figure 3). Despite the apparent perturbation induced by doping, the anisotropy in charge transport[3c] is independent of the $I_2$-position in the pores (Figure 3a and b). For $I_2$ in close proximity of the framework the interaction is sufficiently strong to affect the framework's electronic structure (Figure 3c). The most evident aspect is a significant reduction of the bandgap, even reaching a metallic character for I@4/5. In light of the resolved changes in the UV-vis-NIR spectra that reveal only a modest bandgap narrowing upon doping, the DFT calculations strongly suggest that the dominant dopant configuration is $I_2$@2. Here, the bandgap is 0.616 eV, which is slightly smaller than 0.631 eV for ZnPc-pz. The average effective masses ($m^*$) for holes and electrons of $I_2$@2 are 2.08 and

Final edited form was published in "Journal of the American Chemical Society". 2020, 142 (52), S. 21622–21627. ISSN 1520-5126.
https://doi.org/10.1021/jacs.0c10482

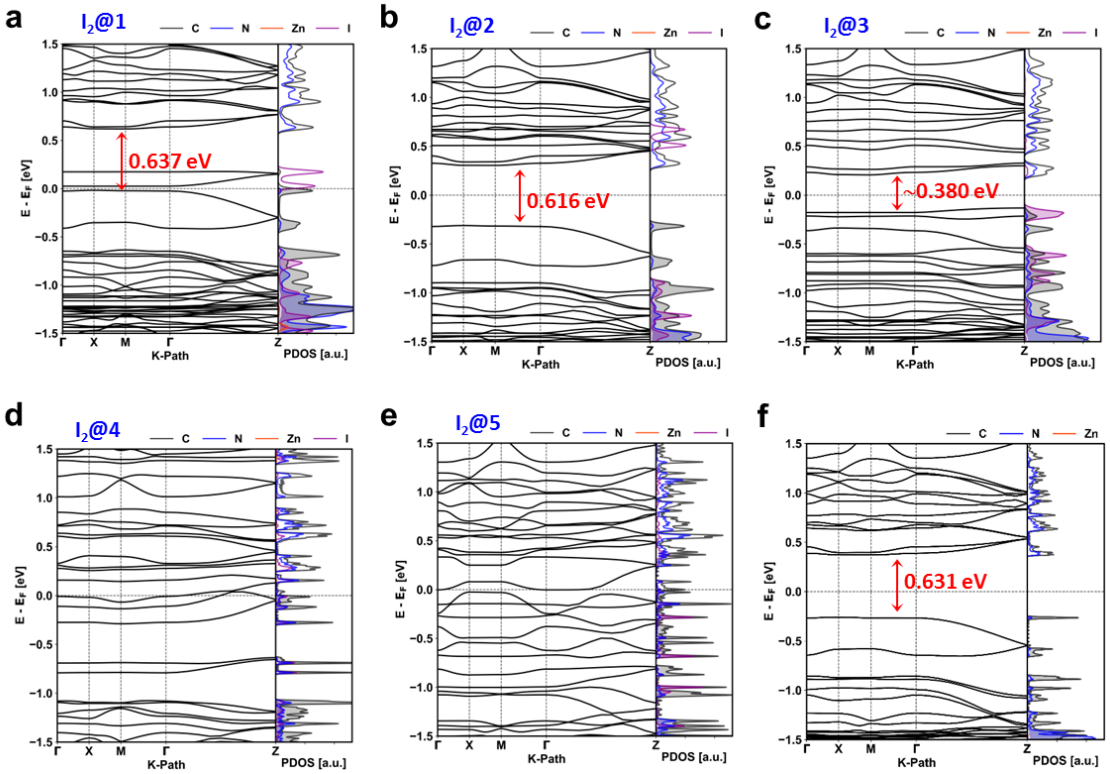


**Figure 3.** Band structures and the projected density of states for **ZnPc-pz-I$_2$**. Pristine ZnPc-pz is shown as reference.[3c]

5.45 $m_0$, respectively (Table S2).

To analyze charge transport in **ZnPc-pz-I$_2$**, we applied Hall effect measurements on compressed pellets at 300 K. The polarity of Hall resistance versus magnetic field reveals a *p*-type semiconducting nature with charge density of ~$9.0\times10^{13}$ cm$^{-3}$ (Figure 4a), which is virtually two orders of magnitude higher than that of ZnPc-pz[3c] and demonstrates the effective doping.[14a,16] Fitting the data provided increased mobility of ~22 cm$^2$/(Vs), that represents a record DC mobility for conductive COFs (Tables S3 and S4).[3c] Since doping does not change $m^*$ (I$_2$@2), the improvement in mobility ($\mu=q^*\tau/m^*$) can be attributed to the increase of scattering time ($\tau$). Based on the charge density and mobility, we infer a conductivity ($\sigma$) of $3.1\times10^{-4}$ S/cm (Table S5). An exponential drop in conductivity upon cooling from 310 to 130 K was found in **ZnPc-pz-I$_2$**; fitting $ln\sigma$ versus $T^{-1}$ (310–230 K) provides an activation energy of 0.21 eV (Figure 4b and Figure S12), smaller than 0.34 eV for ZnPc-pz.[3c] The semi-logarithmic plot of $\sigma$ versus $T^{-1/4}$ over the measured temperature region can be well fitted to the Mott-law variable range hoping model (Figure 4b, inset), indicative of a temperature-dependent hopping conductivity. Moreover, the charge transport depends on the amount of I$_2$. The contrast **ZnPc-pz-I$_2$** sample with 4.7 wt% I$_2$ (Figure S13) exhibited an inferior mobility and conductivity of ~10.5 cm$^2$/(Vs) and ~$5.0\times10^{-5}$ S/cm, respectively. Upon removal of I$_2$, the dedoped sample displayed a significant reduction in conductivity down to ~$8\times10^{-7}$ S/cm (Figure S14), comparable to the undoped ZnPc-pz.[3c] For **CuPc-pz-I$_2$**, Hall mobility and conductivity were obtained as ~7 cm$^2$/(Vs) and ~$1\times10^{-4}$ S/cm, respectively (Figures S15-18).

To further discover the doping effect, we performed TRTS measurements. First, we measured **ZnPc-pz-I$_2$** with below-gap pump excitation; no response was detected (Figure S19), supporting the idea that no metallic phases (I$_2$@4/5) are available in **ZnPc-pz-I$_2$**. Under above-gap excitation, the dynamics are consistent with the ultrafast generation of free charge carriers that follow rapid trapping and/or localization within **ZnPc-pz-I$_2$** (Figure 4c). We noticed that **ZnPc-pz-I$_2$** provides stronger signals than the undoped sample under the same excitation conditions (with up to a 40% increase in peak signal amplitude),[3c] which is consistent with an improved charge mobility. Figure 4d shows the real and imaginary conductivity components versus frequency, measured at the peak of the transient photoconductivity. The data can be well modeled with the Drude-Smith model (shown as solid lines), which accounts for free charge carriers populating the samples that are partially localized via backscattering events. The best fit to the data provides an average scattering time of 66±3 *fs* (average response over 3 samples, Table S6), while for the undoped **ZnPz-pz** the scattering time amounts to ~30 *fs*.[3c] With $m^*$ barely affected by doping, and considering the grain boundary scattering, the THz-mobility of **ZnPc-pz-I$_2$** reaches ~6.3 cm$^2$/(Vs). This figure represents a threefold improvement when compared with mobility resolved for undoped samples of ~2 cm$^2$/(Vs).[3c] These results, in good agreement with Hall effect data, reveal that doping is positively perturbative towards the mobility. This unique phenomenon is related to changes in averaged charge carrier scattering rates in the samples and not due to changes in $m^*$.

In summary, we demonstrate that extrinsic formation of electron-donor-acceptor pairs provides novel route to induce high charge mobility and conductivity in semiconducting 2D *c*-COFs. The charge-transfer complex in **ZnPc-pz-I$_2$** is fully characterized and revealed optically by an additional absorption-peak in the NIR region. Hall effect measurements reveal that doping boosts the carrier density and conductivity in this *p*-type semiconductor. Remarkably, we observed a unique transport phenomenon that doping enhances carrier mobility. With the support of experimental and theoretical characterizations, we can assign the achieved superior mobility to an increased

Final edited form was published in "Journal of the American Chemical Society". 2020, 142 (52), S. 21622–21627. ISSN 1520-5126.
https://doi.org/10.1021/jacs.0c10482

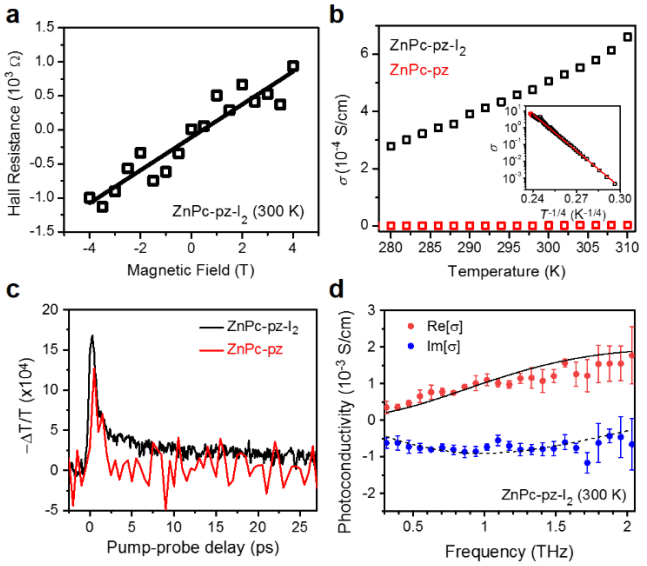


**Figure 4.** Charge transport characterizations. (a) Hall resistance versus field. (b) Variable-temperature $\sigma$ for **ZnPc-pz-I$_2$** (black) and ZnPc-pz[3c] (red). c) Real part of photoconductivity versus pump-probe delay for **ZnPc-pz-I$_2$** (black) and ZnPc-pz[3c] (red). d) Real and imaginary conductivity components of **ZnPc-pz-I$_2$** versus frequency at the peak photoconductivity of (a).

scattering time for the probed free-electrons. Apparently, scattering mechanisms limiting the mobility (e.g. impurity and/or electron-phonon scattering) are suppressed upon doping. Combining DFT simulation and the charge transport properties, we achieve a fundamental understanding about the perturbative dopant role in the electronic structure by establishing reliable structure-electronic property relationships in the synthesized **ZnPc-pz-I$_2$**. Our work paves the way for developing highly conductive COFs by rational doping for (opto)electronic devices.

## ASSOCIATED CONTENT

### Supporting Information

The Supporting Information is available free of charge on the ACS Publications website. Synthetic details, characterization, modelling, and conductivity measurements, and THz experiments (PDF).

## AUTHOR INFORMATION

### Corresponding Author

enrique.canovas@imdea.org
renhao.dong@tu-dresden.de
xinliang.feng@tu-dresden.de

### Author Contributions

⊥These authors contributed equally.

### Notes

The authors declare no competing financial interest.

## ACKNOWLEDGMENT

We thank financial support from EU Graphene Flagship (GrapheneCore3, No. 881603), ERC Grants (T2DCP and FC2DMOF (No. 852909)), H2020-MSCA-ITN (ULTIMATE, No. 813036), DFG projects (COORNETs, SPP 1928 and CRC 1415, No. 417590517), as well as the German Science Council, Center for Advancing Electronics Dresden (EXC1056). We acknowledge Dresden Center for Nanoanalysis (DCN) and Dr. Konrad Schneider (IPF, Dresden) for the use of facilities. We thank Dr. Yanpeng Qi, Dr. Xu-Bing Li, Dr. Wei Li, Dr. Yu Zhang, and Jianfeng Zhang for the helpful discussions. T.H. and H.-H.L. acknowledge the Centre for Information Services and High Performance Computing (ZIH) in Dresden, Germany for the provided computational resources. E.C. acknowledges financial support from the regional government of Comunidad de Madrid under projects 2017-T1/AMB-5207 & P2018/NMT-4511, and the "Severo Ochoa" Programme for Centres of Excellence in R&D (MINECO, Grant No. SEV-2016-0686).

## REFERENCES

(1) (a) Ding, S.-Y.; Gao, J.; Wang, Q.; Zhang, Y.; Song, W.-G.; Su, C.-Y.; Wang, W. Construction of Covalent Organic Framework for Catalysis: Pd/COF-LZU1 in Suzuki–Miyaura Coupling Reaction. *J. Am. Chem. Soc.* **2011,** *133*, 19816-19822. (b) Ascherl, L.; Sick, T.; Margraf, J. T.; Lapidus, S. H.; Calik, M.; Hettstedt, C.; Karaghiosoff, K.; Döblinger, M.; Clark, T.; Chapman, K. W.; Auras, F.; Bein, T. Molecular Docking Sites Sesigned for the Generation of Highly Crystalline Covalent Organic Frameworks. *Nat. Chem.* **2016,** *8*, 310-316. (c) Zhuang, X.; Zhao, W.; Zhang, F.; Cao, Y.; Liu, F.; Bi, S.; Feng, X. A Two-Dimensional Conjugated Polymer Framework with Fully sp2-Bonded Carbon Skeleton. *Polym. Chem.* **2016,** *7*, 4176-4181. (d) Jin, E.; Asada, M.; Xu, Q.; Dalapati, S.; Addicoat, M. A.; Brady, M. A.; Xu, H.; Nakamura, T.; Heine, T.; Chen, Q.; Jiang, D. Two-Dimensional sp2 Carbon–Conjugated Covalent Organic Frameworks. *Science* **2017,** *357*, 673-676. (e) Lyu, H.; Diercks, C. S.; Zhu, C.; Yaghi, O. M. Porous Crystalline Olefin-Linked Covalent Organic Frameworks. *J. Am. Chem. Soc.* **2019,** *141*, 6848-6852.

(2) (a) Mahmood, J.; Lee, E. K.; Jung, M.; Shin, D.; Jeon, I. Y.; Jung, S. M.; Choi, H. J.; Seo, J. M.; Bae, S. Y.; Sohn, S. D.; Park, N.; Oh, J. H.; Shin, H. J.; Baek, J. B. Nitrogenated Holey Two-Dimensional Structures. *Nat. Commun.* **2015,** *6*, 6486. (b) Liu, W.; Luo, X.; Bao, Y.; Liu, Y. P.; Ning, G.-H.; Abdelwahab, I.; Li, L.; Nai, C. T.; Hu, Z. G.; Zhao, D.; Liu, B.; Quek, S. Y.; Loh, K. P. A two-dimensional conjugated aromatic polymer via C–C coupling reaction. *Nat. Chem.* **2017,** *9*, 563-570. (c) Galeotti, G.; De Marchi, F.; Hamzehpoor, E.; MacLean, O.; Rajeswara Rao, M.; Chen, Y.; Besteiro, L. V.; Dettmann, D.; Ferrari, L.; Frezza, F.; Sheverdyaeva, P. M.; Liu, R.; Kundu, A. K.; Moras, P.; Ebrahimi, M.; Gallagher, M. C.; Rosei, F.; Perepichka, D. F.; Contini, G. Synthesis of mesoscale ordered two-dimensional π-conjugated polymers with semiconducting properties. *Nat. Mater.* **2020,** *19*, 874-880. (d) Qi, H.; Sahabudeen, H.; Liang, B.; Položij, M.; Addicoat, M. A.; Gorelik, T. E.; Hambsch, M.; Mundszinger, M.; Park, S.; Lotsch, B. V.; Mannsfeld, S. C. B.; Zheng, Z.; Dong, R.; Heine, T.; Feng, X.; Kaiser, U. Near–atomic-scale observation of grain boundaries in a layer-stacked two-dimensional polymer. *Sci. Adv.* **2020,** *6*, eabb5976. (e) Xu, S.; Wang, G.; Biswal, B. P.; Addicoat, M.; Paasch, S.; Sheng, W.; Zhuang, X.; Brunner, E.; Heine, T.; Berger, R.; Feng, X. A Nitrogen-Rich 2D sp2-Carbon-Linked Conjugated Polymer Framework as a High-Performance Cathode for Lithium-Ion Batteries. *Angew. Chem. Int. Ed.* **2019,** *131*, 859-863.

(3) (a) Guo, J.; Xu, Y.; Jin, S.; Chen, L.; Kaji, T.; Honsho, Y.; Addicoat, M. A.; Kim, J.; Saeki, A.; Ihee, H.; Seki, S.; Irle, S.; Hiramoto, M.; Gao, J.; Jiang, D. Conjugated Organic Framework with Three-Dimensionally Ordered Stable Structure and Delocalized pi Clouds. *Nat. Commun.* **2013,** *4*, 2736. (b) Meng, Z.; Stolz, R. M.; Mirica, K. A. Two-Dimensional Chemiresistive Covalent Organic Framework with High Intrinsic Conductivity. *J. Am. Chem. Soc.* **2019,** *141*, 11929-11937. (c) Wang, M.; Ballabio, M.; Wang, M.; Lin, H.-H.; Biswal, B. P.; Han, X.; Paasch, S.; Brunner, E.; Liu, P.; Chen, M.; Bonn, M.; Heine, T.; Zhou, S.; Cánovas, E.; Dong, R.; Feng, X. Unveiling Electronic Properties in Metal–Phthalocyanine-Based Pyrazine-Linked Conjugated Two-Dimensional Covalent Organic Frameworks. *J. Am. Chem. Soc.* **2019,** *141*, 16810-16816. (d) Li, X.; Wang, H.; Chen, H.; Zheng, Q.; Zhang, Q.; Mao, H.; Liu, Y.; Cai, S.; Sun, B.; Dun, C.; Gordon, M. P.; Zheng, H.; Reimer, J. A.; Urban, J. J.; Ciston, J.; Tan, T.; Chan, E. M.; Zhang, J.; Liu, Y. Dynamic Covalent Synthesis of Crystalline Porous Graphitic Frameworks. *Chem* **2020,** *6*, 933-944.

(4) (a) Kuc, A.; Springer, M. A.; Batra, K.; Juarez-Mosqueda, R.; Wöll, C.; Heine, T. Proximity Effect in Crystalline Framework Materials: Stacking-Induced Functionality in MOFs and COFs. *Adv. Funct. Mater.* **2020,** *30*, 1908004. (b) Dong, R.; Zhang, T.; Feng, X. Interface-Assisted Synthesis of 2D Materials: Trend and Challenges. *Chem. Rev.* **2018,** *118*, 6189-6235.

Final edited form was published in "Journal of the American Chemical Society". 2020, 142 (52), S. 21622–21627. ISSN 1520-5126.
https://doi.org/10.1021/jacs.0c10482

(5) (a) Wu, X.; Han, X.; Xu, Q.; Liu, Y.; Yuan, C.; Yang, S.; Liu, Y.; Jiang, J.; Cui, Y. Chiral BINOL-Based Covalent Organic Frameworks for Enantioselective Sensing. *J. Am. Chem. Soc.* **2019,** *141*, 7081-7089. (b) Liang, R.-R.; Xu, S.-Q.; Zhang, L.; A, R.-H.; Chen, P.; Cui, F.-Z.; Qi, Q.-Y.; Sun, J.; Zhao, X. Rational design of crystalline two-dimensional frameworks with highly complicated topological structures. *Nat. Commun.* **2019,** *10*, 4609.

(6) (a) Biswal, B. P.; Vignolo-González, H. A.; Banerjee, T.; Grunenberg, L.; Savasci, G.; Gottschling, K.; Nuss, J.; Ochsenfeld, C.; Lotsch, B. V. Sustained Solar H2 Evolution from a Thiazolo[5,4-d]thiazole-Bridged Covalent Organic Framework and Nickel-Thiolate Cluster in Water. *J. Am. Chem. Soc.* **2019,** *141*, 11082−11092. (b) Bi, S.; Yang, C.; Zhang, W.; Xu, J.; Liu, L.; Wu, D.; Wang, X.; Han, Y.; Liang, Q.; Zhang, F. Two-dimensional semiconducting covalent organic frameworks via condensation at arylmethyl carbon atoms. *Nat. Commun.* **2019,** *10*, 2467. (c) Zhao, X.; Pachfule, P.; Li, S.; Langenhahn, T.; Ye, M.; Schlesiger, C.; Praetz, S.; Schmidt, J.; Thomas, A. Macro/Microporous Covalent Organic Frameworks for Efficient Electrocatalysis. *J. Am. Chem. Soc.* **2019,** *141*, 6623-6630.

(7) Evans, A. M.; Parent, L. R.; Flanders, N. C.; Bisbey, R. P.; Vitaku, E.; Kirschner, M. S.; Schaller, R. D.; Chen, L. X.; Gianneschi, N. C.; Dichtel, W. R. Seeded Growth of Single-Crystal Two-Dimensional Covalent Organic Frameworks. *Science* **2018,** *361*, 52-57.

(8) (a) Jin, Y.; Hu, Y.; Zhang, W. Tessellated Multiporous Two-Dimensional Covalent Organic Frameworks. *Nature Reviews Chemistry* **2017,** *1*, 0056. (b) Li, Y.; Chen, Q.; Xu, T.; Xie, Z.; Liu, J.; Yu, X.; Ma, S.; Qin, T.; Chen, L. De Novo Design and Facile Synthesis of 2D Covalent Organic Frameworks: A Two-in-One Strategy. *J. Am. Chem. Soc.* **2019,** *141*, 13822-13828.

(9) (a) Biswal, B. P.; Chandra, S.; Kandambeth, S.; Lukose, B.; Heine, T.; Banerjee, R. Mechanochemical Synthesis of Chemically Stable Isoreticular Covalent Organic Frameworks. *J. Am. Chem. Soc.* **2013,** *135*, 5328-5331. (b) Guan, X.; Li, H.; Ma, Y.; Xue, M.; Fang, Q.; Yan, Y.; Valtchev, V.; Qiu, S. Chemically stable polyarylether-based covalent organic frameworks. *Nat. Chem.* **2019,** *11*, 587-594.

(10) (a) Biswal, B. P.; Valligatla, S.; Wang, M.; Banerjee, T.; Saad, N. A.; Mariserla, B. M. K.; Chandrasekhar, N.; Becker, D.; Addicoat, M.; Senkovska, I.; Berger, R.; Rao, D. N.; Kaskel, S.; Feng, X. Nonlinear Optical Switching in Regioregular Porphyrin Covalent Organic Frameworks. *Angew. Chem. Int. Ed.* **2019,** *58*, 6896-6900. (b) Medina, D. D.; Sick, T.; Bein, T. Photoactive and Conducting Covalent Organic Frameworks. *Adv. Energy Mater.* **2017,** *7*, 1700387.

(11) (a) Allendorf, M. D.; Dong, R.; Feng, X.; Kaskel, S.; Matoga, D.; Stavila, V. Electronic Devices Using Open Framework Materials. *Chem. Rev.* **2020,** *120*, 8581–8640. (b) Sun, B.; Zhu, C.-H.; Liu, Y.; Wang, C.; Wan, L.-J.; Wang, D. Oriented Covalent Organic Framework Film on Graphene for Robust Ambipolar Vertical Organic Field-Effect Transistor. *Chem. Mater.* **2017,** *29*, 4367-4374.

(12) Vitaku, E.; Gannett, C. N.; Carpenter, K. L.; Shen, L.; Abruña, H. D.; Dichtel, W. R. Phenazine-Based Covalent Organic Framework Cathode Materials with High Energy and Power Densities. *J. Am. Chem. Soc.* **2020,** *142*, 16-20.

(13) Wan, S.; Gándara, F.; Asano, A.; Furukawa, H.; Saeki, A.; Dey, S. K.; Liao, L.; Ambrogio, M. W.; Botros, Y. Y.; Duan, X.; Seki, S.; Stoddart, J. F.; Yaghi, O. M. Covalent Organic Frameworks with High Charge Carrier Mobility. *Chem. Mater.* **2011,** *23*, 4094-4097.

(14) (a) Wang, L.; Dong, B.; Ge, R.; Jiang, F.; Xu, J. Fluorene-Based Two-Dimensional Covalent Organic Framework with Thermoelectric Properties through Doping. *ACS Appl. Mater.* **2017,** *9*, 7108-7114. (b) Lakshmi, V.; Liu, C.-H.; Rajeswara Rao, M.; Chen, Y.; Fang, Y.; Dadvand, A.; Hamzehpoor, E.; Sakai-Otsuka, Y.; Stein, R. S.; Perepichka, D. F. A Two-Dimensional Poly(azatriangulene) Covalent Organic Framework with Semiconducting and Paramagnetic States. *J. Am. Chem. Soc.* **2020,** *142*, 2155-2160.

(15) Schramm, C. J.; Scaringe, R. P.; Stojakovic, D. R.; Hoffman, B. M.; Ibers, J. A.; Marks, T. J. Chemical, spectral, structural, and charge transport properties of the "molecular metals" produced by iodination of nickel phthalocyanine. *J. Am. Chem. Soc.* **1980,** *102*, 6702-6713.

(16) Bertrand, G. H. V.; Michaelis, V. K.; Ong, T.-C.; Griffin, R. G.; Dincă, M. Thiophene-based covalent organic frameworks. *Proc. Natl. Acad. Sci. U. S. A.*. **2013,** *110*, 4923-4928.

TOC

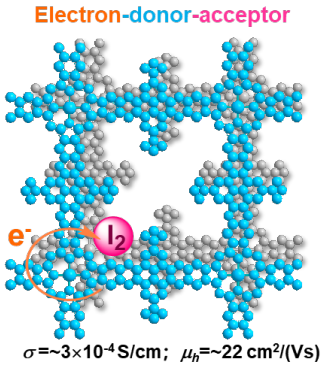




5